THE JOURNAL OF PHYSICAL CHEMISTRY Letters

Letter

Cite This: J. Phys. Chem. Lett. 2019, 10, 3352−3358

pubs.acs.org/JPCL

# Adsorption Features of Formaldehyde on $TiO_2$(110) Surface Probed by High-Resolution Scanning Tunnelling Microscopy

Haochen Wang,[†,∥,▽] Xiangyun Zhao,[†,∥,▽] Chuanqi Huang,[‡,▽] Xianchi Jin,[†,#] Dong Wei,[†] Dongxu Dai,[†] Zhibo Ma,*[,†] Wei-Xue Li,*[,§] and Xueming Yang*[,†,⊥]

[†]State Key Laboratory of Molecular Reaction Dynamics, Dalian Institute of Chemical Physics, Chinese Academy of Science, Dalian, Liaoning 116023, China

[‡]Hangzhou Institute of Advanced Studies, Zhejiang Normal University, Hangzhou, Zhejiang 311231, China

[§]Hefei National Laboratory for Physical Sciences at the Microscale, Department of Chemical Physics, University of Science and Technology of China, Hefei 230026, China

[∥]University of Chinese Academy of Sciences, Beijing 100049, China

[⊥]Department of Chemistry, Southern University of Science and Technology, Shenzhen 518055, China

[#]Scienta Omicron GmbH, Limburger Strasse, 7565232 Taunusstein, Germany



**ABSTRACT:** We report a real-space imaging of formaldehyde (HCHO) adsorption on a $TiO_2$(110) surface probed by high-resolution scanning tunnelling microscopy (STM). Density functional theory calculations (DFT) were carried out to assign the observed features. The adsorptions occur exclusively on 5-fold coordinated Ti ($Ti_{5c}$) sites and oxygen vacancies (OVs). The well-resolved configurations on the $Ti_{5c}$ sites feature the overlapping of the two "dumbbell" structures which are originated from the empty orbitals of HCHO. The STM images for the physical adsorption of HCHO on the OV sites appear fuzzy because of the rapid switching of HCHO among the three stable orientations, while those for the chemical adsorption are much clearer, revealing a distinctive difference between chemical and physical adsorptions. This work presents a systematic characterization of the topological features of HCHO/$TiO_2$(110) and provides useful information for mechanical understanding of the reaction mechanism of HCHO on the surfaces.

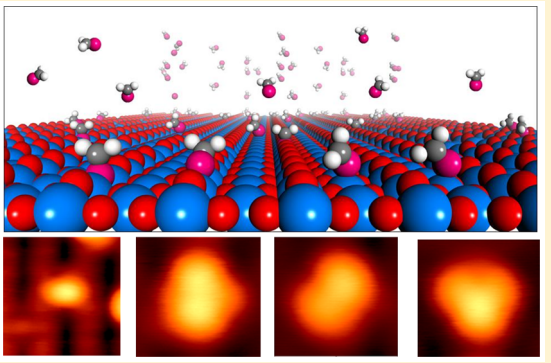

Titanium dioxide ($TiO_2$) is one of the most important materials for catalysis and photocatalysis, especially in water splitting and hydrogen production.[1−11] It has been reported that methanol photoreforming on this surface could produce $H_2$, where formaldehyde (HCHO) has been suggested as a key intermediate.[12−15] Meanwhile, HCHO is a main indoor air pollutant which can be oxidized to $CO_2$ and $H_2O$ by Pt/$TiO_2$ catalysts.[16−23] The $TiO_2$-catalyzed reaction with the involvement of HCHO is relevant to prebiotic syntheses.[24−28] The clarification of the adsorption features of HCHO on $TiO_2$ plays pivotal roles in mechanical understanding the photocatalysis mechanism. Considering that $TiO_2$(110) is the most stable surface with a well-known structure,[10,29] it affords a model substrate for fundamental understanding of the adsorption of HCHO on the surfaces.[10,30,31]

High-resolution scanning tunnelling microscopy has emerged as a powerful technique for probing the molecular orbitals of a single molecule, which contain useful information about adsorption.[32−36] Guo et al. determined the orientation of interfacial water on a NaCl(001) film supported on Au(111) substrate via the analysis of molecular orbital information.[33] Ho and co-workers reported the adsorption details of acetylene on Cu(100), revealing a "dumbbell" shape ascribed to the contribution from a $\pi$ bond.[36]

The adsorption of HCHO on $TiO_2$(110) is still under debate. Theoretical calculation first predicted that an $\eta^2$-dioxymethylene ($\eta^2$ configuration) structure on the $Ti_{5c}$ sites is preferred for the adsorption of HCHO on $TiO_2$(110), while the configurations on oxygen vacancies (OVs) and the $\eta^1$-top adsorption configuration ($\eta^1$ configuration) on $Ti_{5c}$ sites are less stable.[37−39] Although this $\eta^2$ dioxymelthylene, which requires an adsorbed formaldehyde reacting with a bridging surface oxygen, was already confirmed by infrared (IR) spectroscopy,[40,41] this species was not found in the $TiO_2$ system by STM or temperature-programmed desorption (TPD) at the beginning. Zhang et al. used STM to investigate the adsorption and diffusion of HCHO on $TiO_2$(110), and they found OV to be the most stable site.[42] The reaction of HCHO around OV has been investigated thereafter: at 215−

**Received:** February 23, 2019
**Accepted:** June 4, 2019
**Published:** June 4, 2019




DOI: 10.1021/acs.jpclett.9b00522
J. Phys. Chem. Lett. 2019, 10, 3352−3358

300 K, two OV-bound HCHO molecules can be coupled to form Ti-bound ethylene, healing both OV sites. After HCHO exposure at 300 K, the diolate is the majority species on the surface, which is formed by an OV-bound HCHO and a Ti-bound HCHO.[43,44] On the OV-deficient oxidized rutile $TiO_2(110)$ surface, the HCHO tends to be polymerized to yield the paraformaldehyde.[45] Recently, Feng et al. observed the $\eta^2$ configuration using low-bias STM.[46] At 80 K, the $\eta^1$ configuration can be slowly transferred to the $\eta^2$ configuration with a lifetime of about 12 h. They found the transfer is reversible at the experimental conditions of higher bias and higher temperature, which explains the missing $\eta^2$ configuration signal in previous TPD and STM experiments.[42−47]

HCHO has a "fingerprint" dumbbell structure derived from the contribution of a $\pi^*$ bond, which is HCHO's lowest unoccupied molecular orbital (LUMO).[48] It can be resolved at +1.25 V using STM.[48−50] This "fingerprint" may help to reveal further details about configurations and transformations of HCHO on the $TiO_2$ surface. In this work, we systematically studied this "fingerprint" dumbbell shape of HCHO on $TiO_2(110)$ using high-resolution STM, which is supported by density functional theory calculations. Detailed information about HCHO adsorption and transformation on $TiO_2(110)$ is revealed. We also studied the adsorption on OVs, and two distinct images are distinguished. The real-space STM images clearly show an overview of HCHO adsorption on $TiO_2(110)$.

Our theoretical calculation of the adsorption structure on the $Ti_{5c}$ site is consistent with previous work, including physical adsorption and chemical adsorption.[37−39] All the stable structure diagrams are shown in Figure 1a1−d1, and the

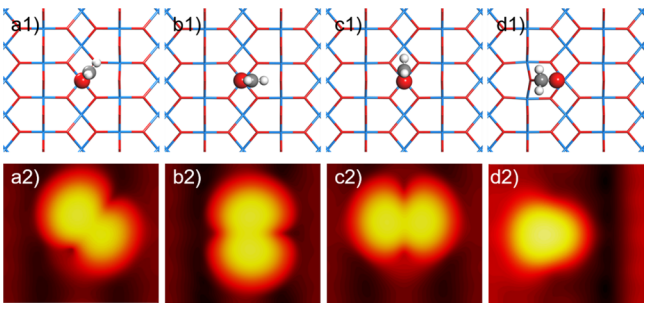


**Figure 1.** DFT calculation and STM simulation of HCHO on $TiO_2(110)$. (a−c) Three types of $\eta^1$ configurations. The C=O bond plane of formaldehyde pointed 52° from the adjacent BBO site, to the adjacent BBO site, and to the $Ti_{5c}$ row, respectively. (a2−c2) In the corresponding STM images, the C=O bond appears as a dividing line in the middle of the protrusion. (d) The carbon atom is connected to the adjacent BBO atom to form a C−O−C bond. Because of the changing of $sp^2$ hybridization, the typical two-piece structure disappeared. Instead, a smaller spot tilted to the BBO row emerged.

adsorption energies are close to the work of Friend et al.[37] The most stable adsorption configuration of HCHO is a chemical adsorption assigned as $\eta^2$-dioxymethylene structure (Figure 1d1) with the adsorption energy of −1.16 eV. The C=O bond of adsorbed HCHO is weakened as compared to that of the free HCHO, leaving the oxygen atom bound to $Ti_{5c}$ and the carbon atom to the adjacent bridging bonded oxygen (BBO) atom. Figure 1a1−c1 presents the HCHO adsorption on the $Ti_{5c}$ row, where HCHO keeps planar with a coordinate bond between the O atom of formaldehyde and the $Ti_{5c}$ site beneath. Configurations with different orientations of the molecular plane relative to BBO row have been explored. The most stable adsorption configuration is shown in Figure 1a1 with its molecular plane tilted by 38° from the $Ti_{5c}$ row. Configuration of HCHO with its molecular plane perpendicular to BBO row is slightly unstable. The parallel configuration, i.e., HCHO molecule parallel to the BBO row, is the most unstable one. The adsorption energies are −0.67, −0.64, and −0.60 eV, respectively.

According to these adsorption configurations, STM images of each structure were simulated as shown in Figure 1a2−d2. We found significant differences between images of physical and chemical adsorptions. The three $\eta^1$ configurations show distinctive two-piece structure. This dumbbell feature originates from HCHO's lowest unoccupied molecular orbital, i.e. its $2\pi^*$ antibonding states, which was discussed in detail in our previous article.[48] The dividing line in the middle of this two-piece structure indicates the orientation of C=O bond. The angle between this dividing line and the bright row indicates the angle between the molecular plane and BBO row, whereas the image of $\eta^2$ configuration is quite different. It shows an oval spot across a bright row and a dark one. The long axis of the spot indicates the orientation of C−O bond. The characteristic of antibonding molecular orbital disappeared because the hybridization of chemisorbed HCHO had already changed, and the molecule bonded to both the Ti and O rows. These features are quite distinct; therefore, every adsorption structure could be easily resolved by STM.

After observing hundreds of molecules adsorbed on $Ti_{5c}$ sites in experiment, three types of adsorption were determined, as shown in Figure 2. Bright rows indicate $Ti_{5c}$ rows, and dark

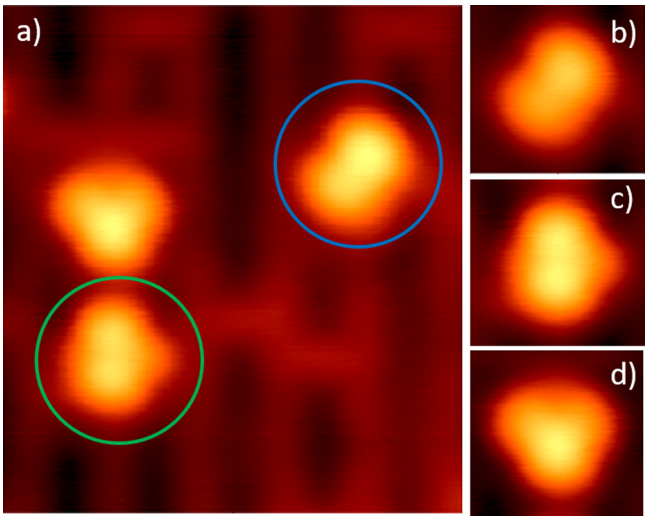


**Figure 2.** STM images of formaldehyde adsorption on the $Ti_{5c}$ sites. (a) Three configurations in real space are observed on the $TiO_2(110)$ (3.4 nm × 3.6 nm, +1.25 V 100 pA). Two $\eta^1$ configuration structures are marked by blue and green circles. (b) The tilted HCHO with a distinct two-piece structure (1.2 nm × 1.1 nm). (c) The C=O bond of HCHO points to the BBO row, and the middle of the dumbbell shape is blurry with a protrusion pointed to one side of the BBO row. (d) A new structure, which is not mentioned in Figure 1.

rows indicate O rows; the bright spots on dark rows are OV sites. Only two $\eta^1$ configurations adsorbed on $Ti_{5c}$ sites are observed and marked by blue and green circles. The tilted HCHO configuration called "dumbbell state" in Figure 2b is consistent with a clear dumbbell shape shown in the simulated image (Figure 1a). Figure 2c shows the case called "cross state"



DOI: 10.1021/acs.jpclett.9b00522
J. Phys. Chem. Lett. 2019, 10, 3352−3358

in which the HCHO's molecular plane is perpendicular to the BBO row. The overall image is similar to Figure 1b. However, on the subject of detail, the dividing line of the dumbbell structure is blurry, and a protrusion extends along the short axis of the overall ellipsoid shape. This protrusion always points to one side of the oxygen row and exists only when the molecular plane is perpendicular to the BBO row; it never exists in the case of the dumbbell state. This seems like the overlap between the features in Figure 1b,d, and we suggest the cross state shows a fast conversion between physical adsorption and chemical adsorption. In Feng et al.'s work,[46] they found that scanning can cause the conversion between $\eta^1$ configuration and $\eta^2$ configuration when bias is higher than +0.75 V, while the $\eta^2$ configuration is not found when the scanning bias is higher than +1.0 V. When the tunnelling electron acts as an activation to trigger HCHO across the energy barrier between two configurations, STM should image the superposition state which contains the features of the two configurations. In this work, the orbital imaging was obtained by the scanning with the bias of +1.25 V, which certainly causes the conversion between the $\eta^1$ configuration and $\eta^2$ configuration (we indeed imaged the overlapping pictures). The bias of +1.25 V is close to the energy of the $2\pi^*$ antibonding states and gave more details to identify this superposition state in imaging, whereas under +1.0 V, the orbital imaging is not favored and the superposition state looks like a featureless bright spot resembling physical adsorption in Feng et al.'s work. The reason why we obtained images of only overlapping states when the molecular plane is perpendicular to the BBO rows might be that the physical adsorption orientation in the cross state is a necessary channel to convert to the chemical adsorption. That is why we never observed this feature in the dumbbell state.

The third image, called the "mouse state" in experiment, is strange (Figure 2d). The image shows three parts, which is obviously different from the $\eta^2$ configuration. It includes one brighter spot and two darker spots. This image is similar to the dumbbell state in some details, as shown in Figure 3. First, if one darker spot is ignored, the angle between the rest and the Ti row is 36°, which is the same as that in the dumbbell state. Furthermore, compared with the heights of different cut profiles, the height and length of the long axis are similar to the dumbbell state; therefore, it was deduced that this feature might originate from HCHO dangling, the $CH_2$ group oscillating toward different BBO rows, and the image represents an overlap of two positions. It is another superposition state between two dumbbell states. However, the trigger of the conversion cannot be temperature or tunnelling electron as the cross state because if that is the case, we can never find a single dumbbell state without overlapping. It can only be attributed to the surface, i.e. the adsorption site, which causes the $CH_2$ oscillation in the mouse state to be different. It is suggested that different types of $Ti_{5c}$ sites around an OV show significant difference in adsorption energy for HCHO on the $TiO_2$(110) surface,[42] and defects on or beneath the surface can also influence the adsorption energy significantly.[37] Therefore, the defects might have substantial effects on the potential energy surfaces for HCHO adsorption on $Ti_{5c}$ sites. On the sites of the mouse state, the energy barrier between two dumbbell states is lower and tunnelling electron can easily trigger the conversion. In contrast, on the sites of the dumbbell state, the barrier is too high for the conversion to be triggered by the tunnelling electron. Another hypothesis is that

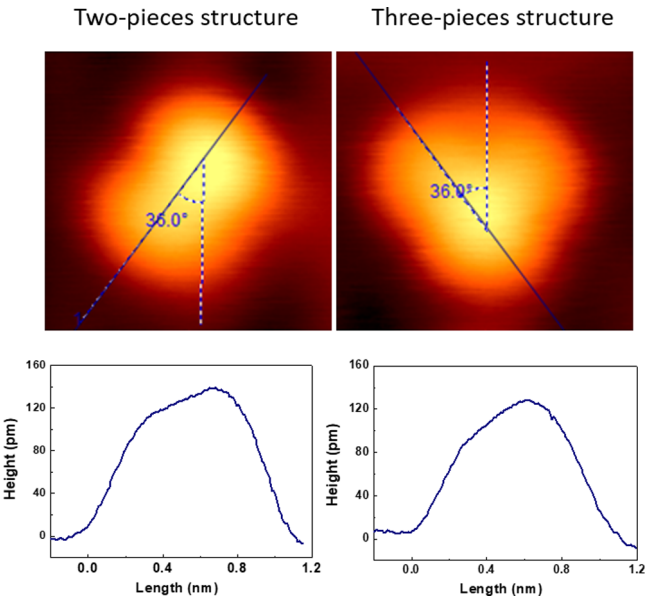


**Figure 3.** Comparison between the tilted formaldehyde and the unknown three-piece structure. The angles between the long axis and $Ti_{5c}$ row are both 36°, and the cut profiles are quite similar.

there are some kinds of activation from the surface, such as polarons. Polarons in rutile can hop to the (110) surface with an energy of tens of millielectronvolts, and its distribution is also site-dependent on the $TiO_2$(110) surface.[51−53] The reason for this conversion under 80 K requires further study in both experiments and calculations.

Under higher temperature, HCHO adsorption will tend to convert to more stable configurations. In Feng et al.'s work, $\eta^1$ configuration has a lifetime of only a few seconds at 105 K and $10^{-5}$ s at 180 K.[46] Under these conditions, the $\eta^1$ configuration will rapidly convert to the $\eta^2$ configuration. They also found that under higher bias, the $\eta^2$ configuration shows a fuzzy feature, suggesting a conversion between physical adsorption and chemical adsorption triggered by tunnelling electrons. However, Zhang et al. found that when the temperature is above 140 K, HCHO will migrate to OV and shows a fuzzy feature when the bias is at +1.3 V.[42] To solve this discrepancy, we heated the surface to 160 K and observed the adsorption configuration of HCHO on the Ti sites. In Figure 4, all the two-piece structures of HCHO molecules are converted to

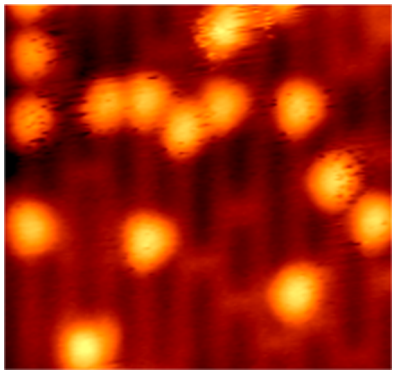

**Figure 4.** STM image of HCHO adsorption under 160 K (6.2 nm × 5.8 nm, +1.25 V 100 pA). The dumbbell structure could not be observed anymore, and most of the protrusions got fuzzy.



DOI: 10.1021/acs.jpclett.9b00522
J. Phys. Chem. Lett. 2019, 10, 3352−3358

fuzzy spots, which are not readily resolved in the STM images. We suggest that it is due to the rapid conversion between all kinds of configurations. Our tunnelling current is 100 pA, which is much larger than that in Feng's experiment. That means the activation rate in the present experiment is much faster, making the conversion of different adsorption configuration so rapid that the images of all configurations are readily overlapped. Our study confirmed that under higher temperature it is possible that HCHO exists on Ti sites.

Besides the $Ti_{5c}$ site, the oxygen vacancy is another general adsorption site. In Figure 5, we listed two distinct structures of

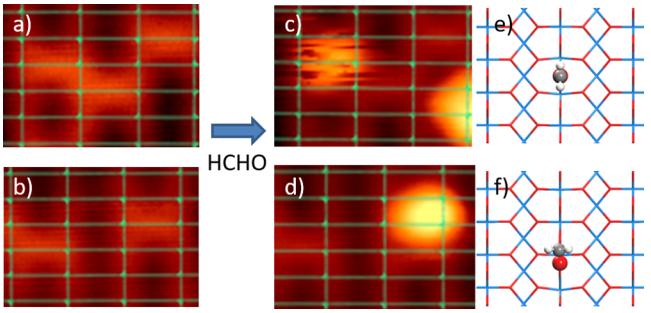


**Figure 5.** STM images of formaldehyde adsorption on the oxygen vacancy sites. (a and b) Bare surface in the in situ experiment. By adding lattice grid, the oxygen vacancies coincide with the green line. (c and d) After HCHO adsorption, two types of HCHO adsorbed on the OV site are observed. The fuzzy spot (c) is on the exact original OV site, but the smooth spot (d) is tilted. (e and f) Optimized adsorption geometries of HCHO binding on the OV site.

the OV sites. The in situ experiment clearly identified that adsorption can occur on/around the OV. Upon addition of a lattice grid, the image in Figure 5c shows a fuzzy protrusion on the exact original OV site. Meanwhile, a smooth type of spot has also been observed, as shown in Figure 5d, whereas this protrusion is slightly tilted in both [001] and [1$\bar{1}$0] directions. In the [001] direction, the protrusion does not reside on the original OV site. Instead, it is near the adjacent bridging oxygen site. In previous calculations, there are two kinds of stable adsorption configurations existing on the OV. In Figure 5e, the oxygen of HCHO is filled into the oxygen vacancy with the $CH_2$ group standing upright. Another stable structure is a chemical adsorption in which one of the C=O bonds is weakened and the C atom of HCHO binds to the adjacent bridging bonded oxygen. Therefore, the diagram of this structure is between the original vacancy and the adjacent oxygen atom, as shown in Figure 5f. Considering the obvious difference between the two molecule positions, panels e and f of Figure 5 correspond to the structures of the protrusions in panels c and d of Figure 5, representing physical and chemical adsorptions on OV, respectively.

With further investigation of the physical adsorption's fuzzy behavior, we found that it strongly depends on the scanning parameter, as Zhang et al. have reported.[44] We did detailed experiments to explore the connection between the feature and the scanning parameter. Figure 6 shows a series of STM images of HCHO adsorbed on the OV sites with different imaging conditions. When we decreased the voltage to +1 V with the same tunnelling current, the protrusion on the OV changed to a stable bright spot. This protrusion tilted to the left side of the original OV site (Figure 6b). The fuzzy character reappeared after the scanning voltage was turned back to +1.25 V (Figure 6c). When the voltage changed to +1 V once again, another stable feature with the location of this protrusion moving to the right of the oxygen vacancy was observed (Figure 6d). However, after the voltage was switched one more time, the protrusion was stabilized at the original OV site. The pattern of the bright feature is similar to H on the BBO site (Figure 6f).[54] In various trials, only these three kinds of stable protrusions are observed. Considering the left and right ones are symmetrical, actually there are only two stable structures. We suggest that different orientations are derived from the $CH_2$ group. In the left and right ones, the $CH_2$ group points to one side of the

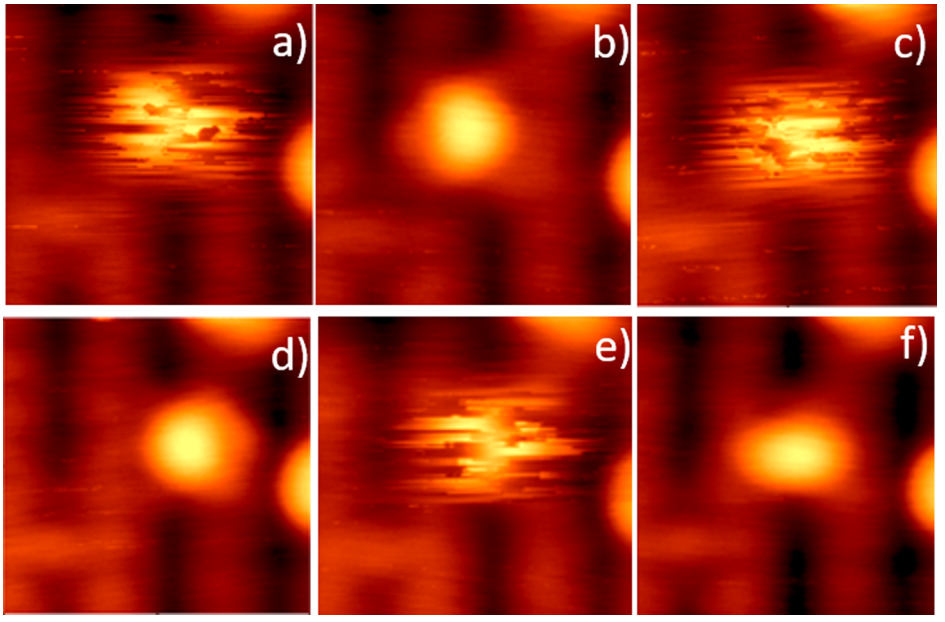


**Figure 6.** Switch between fuzzy and stable characters (1.7 nm × 1.7 nm). (a, c, and e) The fuzzy feature of HCHO adsorbed on the OV site under +1.25 V and 100 pA. When the scanning voltage decreased to +1.0 V, the protrusion became stable, and panels b, d, and f are three distinct protrusions on different positions relative to the original OV site.



DOI: 10.1021/acs.jpclett.9b00522
J. Phys. Chem. Lett. 2019, 10, 3352−3358

BBO rows, whereas in the case of Figure 6f, the $CH_2$ stands upright. The fuzzy feature represents the conversion between these physical adsorption states under higher bias. The conversion rate on the OV might be too low, compared to that on $Ti_{5c}$ sites, to image a state superposition behavior, and only fuzzy lines can be obtained.

We have systematically investigated the adsorption of HCHO on the reduced $TiO_2$(110) surface. New distinctive adsorption features were observed, which were identified with the combination of STM techniques and DFT calculations. The mouse state and the cross state appear on the $Ti_{5c}$ sites. The physical adsorption and chemical adsorption are distinguished on the OV sites. The results afford a clarification of the adsorption features of HCHO on $TiO_2$, which should have important implications for the mechanical understanding of the photocatalysis mechanism.

## METHODS

Experiments were performed in an ultrahigh vacuum (UHV) low-temperature (LT) STM (Matrix, Omicron). Because low partial pressure of water has a severe impact on the HCHO/$TiO_2$(110) system, the whole chamber was baked out for 80 h to eliminate water. The base pressure is better than $4 \times 10^{-11}$ mbar. The $TiO_2$(110) (Princeton Scientific, $10 \times 5 \times 1$ $mm^3$) was prepared by repeated cycles of $Ar^+$ ion sputtering (1 keV, 1.5 $\mu$A, 10 min) and UHV annealing (850 K, 20 min). A clean reduced $TiO_2$(110)-$(1 \times 1)$ surface was obtained and checked by STM. Formaldehyde was generated via thermal decomposition of paraformaldehyde (Sigma-Aldrich, 95% purity), which was purified via several heat−freeze−pump−thaw cycles. Formaldehyde was then introduced into the chamber by a homemade doser. The sample was cooled to 80 K by liquid nitrogen. The tip was retracted about 20 $\mu$m from the surface to avoid the shadow effect while dosing.

DFT calculations were performed using the Vienna ab initio simulation package (VASP)[55,56] based on the projected augmented wave (PAW) method[57,58] with the GGA and the spin polarized Perdew−Burke−Ernzerhof (PBE) exchange−correlation functional.[59] A plane wave basis set with kinetic energy cutoff of 400 eV was used to solve the Kohn−Sham equations. A periodic slab of six Ti layers cut out of $TiO_2$ crystal separated by a 16 Å vacuum gap was used to model the $TiO_2$(110) surface. The bottom two layers were fixed to the bulk structure, and upper layers were relaxed until the force acting on each atom was less than 0.03 eV/Å. A Γ-point and Monhkorst−Pack grid of $(2 \times 2 \times 1)$ for a $4 \times 2$ surface unit cell was used for the structure optimization and the electronic structure calculations, respectively. The STM images were simulated on the basis of Tersoff and Hamann's formula[60,61] using the bSKAN code.[62]

## AUTHOR INFORMATION


### Corresponding Authors

*E-mail: zhbma@dicp.ac.cn (Z.M.).
*E-mail: wxli70@ustc.edu.cn (W.-X.L.).
*E-mail: xmyang@dicp.ac.cn. Tel: +86-411-84695174. Fax: +86-411-84675584 (X.Y.).

### ORCID

Haochen Wang: 0000-0003-0234-7932
Wei-Xue Li: 0000-0002-5043-3088

### Author Contributions

[∇]H.W., X.Z., and C.H. contributed equally to this work.


### Notes

The authors declare no competing financial interest.

## ACKNOWLEDGMENTS

The authors acknowledge financial support from the National Natural Science Foundation of China (Grants 21673236, 21688102, and 91645202), the Strategic Priority Research Program of Chinese Academy of Science (Grants XDB17000000 and QYZDJ-SSW-SLH054), and the National Key Research and Development Program of the MOST of China (Grants 2016YFA0200603, 2017YFB0602205, and 2018YFA0208603). We appreciate the insightful suggestions of Prof. Wang Bing and Dr. Tan Shijing regarding the equipment's design and installation.

## REFERENCES


(1) Fujishima, A.; Honda, K. Electrochemical Photolysis of Water at a Semiconductor Electrode. *Nature* **1972**, *238* (5358), 37.
(2) Asahi, R.; Morikawa, T.; Ohwaki, T.; Aoki, K.; Taga, Y. Visible-Light Photocatalysis in Nitrogen-Doped Titanium Oxides. *Science* **2001**, *293* (5528), 269−271.
(3) Maeda, K.; Domen, K. Photocatalytic Water Splitting: Recent Progress and Future Challenges. *J. Phys. Chem. Lett.* **2010**, *1* (18), 2655−2661.
(4) Khan, S. U. M.; Al-Shahry, M.; Ingler, W. B. Efficient Photochemical Water Splitting by a Chemically Modified n-$TiO_2$. *Science* **2002**, *297* (5590), 2243−2245.
(5) Youngblood, W. J.; Lee, S. H. A.; Maeda, K.; Mallouk, T. E. Visible Light Water Splitting Using Dye-Sensitized Oxide Semiconductors. *Acc. Chem. Res.* **2009**, *42* (12), 1966−1973.
(6) Wahlstrom, E.; Vestergaard, E. K.; Schaub, R.; Ronnau, A.; Vestergaard, M.; Laegsgaard, E.; Stensgaard, I.; Besenbacher, F. Electron Transfer-Induced Dynamics of Oxygen Molecules on the $TiO_2$(110). *Science* **2004**, *303* (5657), 511−513.
(7) Osterloh, F. E. Inorganic Materials as Catalysts for Photochemical Splitting of Water. *Chem. Mater.* **2008**, *20* (1), 35−54.
(8) Maeda, K.; Domen, K. New Non-Oxide Photocatalysts Designed for Overall Water Splitting under Visible Light. *J. Phys. Chem. C* **2007**, *111* (22), 7851−7861.
(9) Fox, M. A.; Dulay, M. T. Heterogeneous Photocatalysis. *Chem. Rev.* **1993**, *93* (1), 341−357.
(10) Linsebigler, A. L.; Lu, G. Q.; Yates, J. T. Photocatalysis on $TiO_2$ Surfaces-Principles, Mechanisms and Selected Results. *Chem. Rev.* **1995**, *95* (3), 735−758.
(11) Fujishima, A.; Zhang, X.; Tryk, D. A. $TiO_2$ Photocatalysis and Related Surface Phenomena. *Surf. Sci. Rep.* **2008**, *63* (12), 515−582.
(12) Kawai, T.; Sakata, T. Photocatalytic Hydrogen-Production from Liquid Methanol and Water. *J. Chem. Soc., Chem. Commun.* **1980**, No. 15, 694−695.
(13) Wang, C. Y.; Rabani, J.; Bahnemann, D. W.; Dohrmann, J. K. Photonic Efficiency and Quantum Yield of Formaldehyde Formation from Methanol in the Presence of Various $TiO_2$ Photocatalysts. *J. Photochem. Photobiol., A* **2002**, *148* (1−3), 169−176.
(14) Yamakata, A.; Ishibashi, T.; Onishi, H. Electron- and Hole-Capture Reactions on Pt/$TiO_2$ Photocatalyst Exposed to Methanol Vapor Studied with Time-Resolved Infrared Absorption Spectroscopy. *J. Phys. Chem. B* **2002**, *106* (35), 9122−9125.
(15) Cui, W. Q.; Feng, L. R.; Xu, C. H.; Lu, S. J.; Qiu, F. Hydrogen Production by Photocatalytic Decomposition of Methanol Gas on Pt/$TiO_2$ Nano-Film. *Catal. Commun.* **2004**, *5* (9), 533−536.
(16) Zhang, C.; He, H. A Comparative Study of $TiO_2$ Supported Noble Metal Catalysts for the Oxidation of Formaldehyde at Room Temperature. *Catal. Today* **2007**, *126* (3−4), 345−350.
(17) Zhang, C. B.; He, H.; Tanaka, K. Perfect Catalytic Oxidation of Formaldehyde over a Pt/$TiO_2$ Catalyst at Room Temperature. *Catal. Commun.* **2005**, *6* (3), 211−214.




DOI: 10.1021/acs.jpclett.9b00522
J. Phys. Chem. Lett. 2019, 10, 3352−3358

(18) Zhang, C. B.; Liu, F. D.; Zhai, Y. P.; Ariga, H.; Yi, N.; Liu, Y. C.; Asakura, K.; Flytzani-Stephanopoulos, M.; He, H. Alkali-Metal-Promoted Pt/$TiO_2$ Opens a More Efficient Pathway to Formaldehyde Oxidation at Ambient Temperatures. *Angew. Chem., Int. Ed.* **2012**, *51* (38), 9628−9632.
(19) Huang, H. B.; Leung, D. Y. C. Complete Elimination of Indoor Formaldehyde over Supported Pt Catalysts with Extremely Low Pt Content at Ambient Temperature. *J. Catal.* **2011**, *280* (1), 60−67.
(20) Huang, H. B.; Leung, D. Y. C.; Ye, D. Q. Effect of Reduction Treatment on Structural Properties of $TiO_2$ Supported Pt Nanoparticles and Their Catalytic Activity for Formaldehyde Oxidation. *J. Mater. Chem.* **2011**, *21* (26), 9647−9652.
(21) Chen, H. Y.; Tang, M. N.; Rui, Z. B.; Ji, H. B. $MnO_2$ Promoted $TiO_2$ Nanotube Array Supported Pt Catalyst for Formaldehyde Oxidation with Enhanced Efficiency. *Ind. Eng. Chem. Res.* **2015**, *54* (36), 8900−8907.
(22) Cui, G. X.; Xin, Y.; Jiang, X.; Dong, M. Q.; Li, J. L.; Wang, P.; Zhai, S. M.; Dong, Y. C.; Jia, J. B.; Yan, B. Safety Profile of $TiO_2$-Based Photocatalytic Nanofabrics for Indoor Formaldehyde Degradation. *Int. J. Mol. Sci.* **2015**, *16* (11), 27721−27729.
(23) Curcio, M. S.; Oliveira, M. P.; Waldman, W. R.; Sanchez, B.; Canela, M. C. $TiO_2$ Sol-Gel for Formaldehyde Photodegradation Using Polymeric Support: Photocatalysis Efficiency Versus Material Stability. *Environ. Sci. Pollut. Res.* **2015**, *22* (2), 800−809.
(24) Civis, S.; Szabla, R.; Szyja, B. M.; Smykowski, D.; Ivanek, O.; Knizek, A.; Kubelik, P.; Sponer, J.; Ferus, M.; Sponer, J. E. $TiO_2$-Catalyzed Synthesis of Sugars from Formaldehyde in Extraterrestrial Impacts on the Early Earth. *Sci. Rep.* **2016**, *6*, 23199.
(25) Saladino, R.; Crestini, C.; Costanzo, G.; Negri, R.; Di Mauro, E. A Possible Prebiotic Synthesis of Purine, Adenine, Cytosine, and 4(3H)-Pyrimidinone from Formamide: Implications for the Origin of Life. *Bioorg. Med. Chem.* **2001**, *9* (5), 1249−1253.
(26) Saladino, R.; Ciambecchini, U.; Crestini, C.; Costanzo, G.; Negri, R.; Di Mauro, E. One-Pot TiO2-Catalyzed Synthesis of Nucleic Bases and Acyclonucleosides from Formamide: Implications for the Origin of Life. *ChemBioChem* **2003**, *4* (6), 514−521.
(27) Saladino, R.; Crestini, C.; Costanzo, G.; DiMauro, E. Advances in the Prebiotic Synthesis of Nucleic Acids Bases: Implications for the Origin of Life. *Curr. Org. Chem.* **2004**, *8* (15), 1425−1443.
(28) Senanayake, S. D.; Idriss, H. Photocatalysis and the Origin of Life: Synthesis of Nucleoside Bases from Formamide on $TiO_2$(001) Single Surfaces. *Proc. Natl. Acad. Sci. U. S. A.* **2006**, *103* (5), 1194−1198.
(29) Diebold, U. The Surface Science of Titanium Dioxide. *Surf. Sci. Rep.* **2003**, *48* (5−8), 53−229.
(30) Wang, Y.; Woell, C. IR Spectroscopic Investigations of Chemical and Photochemical Reactions on Metal Oxides: Bridging the Materials Gap. *Chem. Soc. Rev.* **2017**, *46* (7), 1875−1932.
(31) Wang, Y.; Woell, C. Chemical Reactions on Metal Oxide Surfaces Investigated by Vibrational Spectroscopy. *Surf. Sci.* **2009**, *603* (10−12), 1589−1599.
(32) Jiang, Y.; Huan, Q.; Fabris, L.; Bazan, G. C.; Ho, W. Submolecular Control, Spectroscopy and Imaging of Bond-Selective Chemistry in Single Functionalized Molecules. *Nat. Chem.* **2013**, *5* (1), 36−41.
(33) Guo, J.; Meng, X. Z.; Chen, J.; Peng, J. B.; Sheng, J. M.; Li, X. Z.; Xu, L. M.; Shi, J. R.; Wang, E. G.; Jiang, Y. Real-Space Imaging of Interfacial Water with Submolecular Resolution. *Nat. Mater.* **2014**, *13* (2), 184−189.
(34) Gross, L.; Moll, N.; Mohn, F.; Curioni, A.; Meyer, G.; Hanke, F.; Persson, M. High-Resolution Molecular Orbital Imaging Using a p-Wave STM Tip. *Phys. Rev. Lett.* **2011**, *107* (8), 086101.
(35) Liljeroth, P.; Repp, J.; Meyer, G. Current-Induced Hydrogen Tautomerization and Conductance Switching of Naphthalocyanine Molecules. *Science* **2007**, *317* (5842), 1203−1206.
(36) Stipe, B. C.; Rezaei, M. A.; Ho, W. Single-Molecule Vibrational Spectroscopy and Microscopy. *Science* **1998**, *280* (5370), 1732−1735.
(37) Haubrich, J.; Kaxiras, E.; Friend, C. M. The Role of Surface and Subsurface Point Defects for Chemical Model Studies on $TiO_2$: a First-Principles Theoretical Study of Formaldehyde Bonding on Rutile $TiO_2$(110). *Chem. - Eur. J.* **2011**, *17* (16), 4496−4506.
(38) Liu, H.; Wang, X.; Pan, C.; Liew, K. M. First-Principles Study of Formaldehyde Adsorption on $TiO_2$ Rutile (110) and Anatase (001) Surfaces. *J. Phys. Chem. C* **2012**, *116* (14), 8044−8053.
(39) Liu, L.; Zhao, J. Formaldehyde Adsorption and Decomposition on Rutile (110): A First-Principles Study. *Surf. Sci.* **2016**, *652*, 156−162.
(40) Onishi, T.; Abe, H.; Maruya, K.-i.; Domen, K. Surface Species Formed from the Reaction of $H_2$−CO over $ZrO_2$ as Studied by IR Spectroscopy. *J. Chem. Soc., Chem. Commun.* **1986**, *2*, 103−104.
(41) Idriss, H.; Hindermann, J.; Kieffer, R.; Kiennemann, A.; Vallet, A.; Chauvin, C.; Lavalley, J.; Chaumette, P. Characterization of Dioxymethylene Species over Cu-Zn Catalysts. *J. Mol. Catal.* **1987**, *42* (2), 205−213.
(42) Zhang, Z.; Tang, M.; Wang, Z.-T.; Ke, Z.; Xia, Y.; Park, K. T.; Lyubinetsky, I.; Dohnálek, Z.; Ge, Q. Imaging of Formaldehyde Adsorption and Diffusion on $TiO_2$(110). *Top. Catal.* **2015**, *58* (2−3), 103−113.
(43) Zhu, K.; Xia, Y. B.; Tang, M. R.; Wang, Z. T.; Lyubinetsky, I.; Ge, Q. F.; Dohnalek, Z.; Park, K. T.; Zhang, Z. R. Low-Temperature Reductive Coupling of Formaldehyde on Rutile $TiO_2$(110). *J. Phys. Chem. C* **2015**, *119* (32), 18452−18457.
(44) Zhu, K.; Xia, Y. B.; Tang, M. R.; Wang, Z. T.; Jan, B.; Lyubinetsky, I.; Ge, Q. F.; Dohnalek, Z.; Park, K. T.; Zhang, Z. R. Tracking Site-Specific C-C Coupling of Formaldehyde Molecules on Rutile $TiO_2$(110). *J. Phys. Chem. C* **2015**, *119* (25), 14267−14272.
(45) Yu, X. J.; Zhang, Z. R.; Yang, C. W.; Bebensee, F.; Heissler, S.; Nefedov, A.; Tang, M. R.; Ge, Q. F.; Chen, L.; Kay, B. D.; Dohnalek, Z.; Wang, Y. M.; Woll, C. Interaction of Formaldehyde with the Rutile $TiO_2$(110) Surface: a Combined Experimental and Theoretical Study. *J. Phys. Chem. C* **2016**, *120* (23), 12626−12636.
(46) Feng, H.; Liu, L.; Dong, S.; Cui, X.; Zhao, J.; Wang, B. Dynamic Processes of Formaldehyde at Terminal Ti Sites on the Rutile $TiO_2$(110) Surface. *J. Phys. Chem. C* **2016**, *120* (42), 24287−24293.
(47) Xu, C.; Yang, W.; Guo, Q.; Dai, D.; Minton, T. K.; Yang, X. Photoinduced Decomposition of Formaldehyde on a $TiO_2$(110) Surface, Assisted by Bridge-Bonded Oxygen Atoms. *J. Phys. Chem. Lett.* **2013**, *4* (16), 2668−2673.
(48) Wei, D.; Jin, X.; Huang, C.; Dai, D.; Ma, Z.; Li, W.-X.; Yang, X. Direct Imaging Single Methanol Molecule Photocatalysis on Titania. *J. Phys. Chem. C* **2015**, *119* (31), 17748−17754.
(49) Guan, D. W.; Wang, R. M.; Jin, X. C.; Dai, D. X.; Ma, Z. B.; Fan, H. J.; Yang, X. M. Diffusion of Formaldehyde on Rutile $TiO_2$(110) Assisted by Surface Hydroxyl Groups. *Chin. J. Chem. Phys.* **2017**, *30* (3), 253−258.
(50) Jin, X.; Li, C.; Xu, C.; Guan, D.; Cheruvathur, A.; Wang, Y.; Xu, J.; Wei, D.; Xiang, H.; Niemantsverdriet, J. W.; Li, Y.; Guo, Q.; Ma, Z.; Su, R.; Yang, X. Photocatalytic C-C Bond Cleavage in Ethylene Glycol on $TiO_2$: A Molecular Level Picture and the Effect of Metal Nanoparticles. *J. Catal.* **2017**, *354*, 37−45.
(51) Setvin, M.; Franchini, C.; Hao, X.; Schmid, M.; Janotti, A.; Kaltak, M.; Van de Walle, C. G.; Kresse, G.; Diebold, U. Direct View at Excess Electrons in $TiO_2$ Rutile and Anatase. *Phys. Rev. Lett.* **2014**, *113* (8), 086402.
(52) Yim, C. M.; Watkins, M. B.; Wolf, M. J.; Pang, C. L.; Hermansson, K.; Thornton, G. Engineering Polarons at a Metal Oxide Surface. *Phys. Rev. Lett.* **2016**, *117* (11), 116402.
(53) Reticcioli, M.; Setvin, M.; Schmid, M.; Diebold, U.; Franchini, C. Formation And Dynamics of Small Polarons on the Rutile $TiO_2$(110) Surface. *Phys. Rev. B: Condens. Matter Mater. Phys.* **2018**, *98* (4), 045306.
(54) Zhang, Z. R.; Bondarchuk, O.; White, J. M.; Kay, B. D.; Dohnalek, Z. Imaging Adsorbate O-H Bond Cleavage: Methanol on $TiO_2$(110). *J. Am. Chem. Soc.* **2006**, *128* (13), 4198−4199.
(55) Kresse, G.; Furthmuller, J. Efficient Iterative Schemes for Ab Initio Total-Energy Calculations Using a Plane-Wave Basis Set. *Phys. Rev. B: Condens. Matter Mater. Phys.* **1996**, *54* (16), 11169−11186.


DOI: 10.1021/acs.jpclett.9b00522
J. Phys. Chem. Lett. 2019, 10, 3352−3358

(56) Kresse, G.; Furthmuller, J. Efficiency of Ab-Initio Total Energy Calculations for Metals and Semiconductors Using a Plane-Wave Basis Set. *Comput. Mater. Sci.* **1996**, *6* (1), 15−50.
(57) Blochl, P. E. Projector Augmented-Wave Method. *Phys. Rev. B: Condens. Matter Mater. Phys.* **1994**, *50* (24), 17953−17979.
(58) Kresse, G.; Joubert, D. From Ultrasoft Pseudopotentials to the Projector Augmented-Wave Method. *Phys. Rev. B: Condens. Matter Mater. Phys.* **1999**, *59* (3), 1758−1775.
(59) Perdew, J. P.; Burke, K.; Ernzerhof, M. Generalized Gradient Approximation Made Simple. *Phys. Rev. Lett.* **1996**, *77* (18), 3865−3868.
(60) Tersoff, J.; Hamann, D. R. Theory and Application for the Scanning Tunneling Microscope. *Phys. Rev. Lett.* **1983**, *50* (25), 1998−2001.
(61) Tersoff, J.; Hamann, D. R. Theory of the Scanning Tunneling Microscope. *Phys. Rev. B: Condens. Matter Mater. Phys.* **1985**, *31* (2), 805−813.
(62) Hofer, W. A. Challenges and Errors: Interpreting High Resolution Images in Scanning Tunneling Microscopy. *Prog. Surf. Sci.* **2003**, *71* (5−8), 147−183.



DOI: 10.1021/acs.jpclett.9b00522
*J. Phys. Chem. Lett.* 2019, 10, 3352−3358